metals

MDPI

Communication

Grain Refinement of Ti-15Mo-3Al-2.7Nb-0.2Si Alloy with the Rotation of TiB Whiskers by Powder Metallurgy and Canned Hot Extrusion

Jiabin Hou [1,2], Lin Gao [1], Guorong Cui [1,*], Wenzhen Chen [1], Wencong Zhang [1] and Wenguang Tian [3]

[1] School of Materials Science and Engineering, Harbin Institute of Technology, Weihai 264209, China; houjiabinwh@163.com (J.H.); gaolinhit@hotmail.com (L.G.); nclwens@hit.edu.cn (W.C.); zwinc@hitwh.edu.cn (W.Z.)
[2] Naval Architecture and Marine Engineering College, Shandong Jiaotong University, Weihai 264209, China
[3] Oriental Bluesky Titanium Technology Co., LTD, Yantai 264003, China; tianwenguang@obtc.cn
* Correspondence: cuiguorong2010@126.com; Tel.: +86-631-5687209

Received: 8 December 2019; Accepted: 12 January 2020; Published: 15 January 2020

Abstract: In situ synthesized TiB whiskers (TiBw) reinforced Ti-15Mo-3Al-2.7Nb-0.2Si alloys were successfully manufactured by pre-sintering and canned hot extrusion via adding TiB_2 powders. During pre-sintering, most TiB_2 were reacted with Ti atoms to produce TiB. During extrusion, the continuous dynamic recrystallization (CDRX) of β grains was promoted with the rotation of TiBw, and CDRXed grains were strongly inhibited by TiBw with hindering dislocation motion. Eventually, the grain sizes of composites decreased obviously. Furthermore, the stress transmitted from the matrix to TiBw for strengthening in a tensile test, besides grain refinement. Meanwhile, the fractured TiBw and microcracks around them contributed to fracturing.

Keywords: TiB whiskers; dynamic recrystallization; grain refinement; strengthening

1. Introduction

Metastable β titanium alloys such as Ti-15Mo-3Al-2.7Nb-0.2Si are a promising candidate applied in aerospace and automotive industries, which have the advantages of high specific strength, excellent hot and cold workability, deep hardenability and oxidation resistance [1–3]. However, during hot working, metastable β titanium alloys coarsen rapidly at elevated temperatures, which could weaken their thermal stability and mechanical properties [4]. Therefore, it is necessary to reduce the grain sizes of metastable β titanium alloys and restrict their growth. In order to overcome the drawback, lots of studies about beta-titanium alloys reinforced by intermetallic particles (or eutectic structures) were carried out [5–12]. The Ni and Co elements were partially segregated to the interdendritic region to form TiNi and TiCo intermetallic phases, resulting in fine interdendritic precipitates or eutectic structures to obtain high strength [5–7,13]. Meanwhile, TiBw was considered to be one of the best reinforcements for Ti matrix with high elastic modulus, clean bonding interface and similar thermal expansion coefficient with matrix [14]. Huang et al. [15] reported that the accumulation of strain around TiBw provided a nucleation site for dynamic recrystallization (DRX) in hot deformation process, which results in some small and fine α of Ti60. Moreover, Feng et al. [16] reported that the growth of the recrystallization primary β was strongly restricted by the TiBw during the extrusion process, which reduced the grain sizes of Ti64. Okulov et al. [17] reported that multicomponent Ti alloys was refined by adding boron during casting. The TiB needle-shape particles distributed along primary β-Ti dendrites, and reduced the secondary dendrite arm spacing of the β-Ti phase, resulting in grain refinement. At present, there are fewer scholars researching metastable β titanium alloys reinforced by

TiBw (TiBw/metastable β titanium) in the hot deformation process, particularly the grain refinement mechanism of TiBw/metastable β titanium.

The grain-refinement mechanism of TiBw/Ti-15Mo-3Al-2.7Nb-0.2Si is worthy of exploring. Above all, composites were fabricated by low energy milling, pre-sintering and canned hot extrusion via adding 2.6 vol % TiB_2.

2. Materials and Methods

The spherical Ti-15Mo-3Al-2.7Nb-0.2Si (alloy) powders (β transus ~ 827 °C) and prismatic TiB_2 powders were chosen as raw materials to produce the as-extruded bars of TiBw reinforced alloys (composites) and alloys. Alloy powders were approximately 120 μm, and TiB_2 powders were approximately 3 μm. Alloy powders (97.4 vol %) and TiB_2 powders (2.6 vol %) were mixed at a speed of 100 rpm for a period of 6 h by low energy milling (LEM) in a planetary ball mill under the protective atmosphere of argon. The weight ratio between balls and powder mixture was 5:1. The mixed powders and alloy powders were weld-sealed into a 45# steel cup (with dimensions of 52 mm in outside diameter, 40 mm in inside diameter, 50 mm in height) [16]. Then billets were pre-sintered in high-temperature box furnace at 1100 °C for 1 h and then cooled by air to room temperature. The pre-sintered billets were heated at 800, 900 and 1000 °C for 30 min and then subsequently extruded by hydraulic machine, with the extrusion ratio of 10.6:1. The as-extruded bars with a diameter of 16 mm and a length of 500 mm were obtained.

The Phases of composites were identified by X-ray diffraction (XRD) (Rigaku Corporation, Tokyo, Japan). The microstructure was observed by scanning electron microscopy (SEM) (Zeiss-MERLIN, Zürich, Switzerland) and equipped with electron back scattered diffraction (EBSD) system. The tensile specimens with gauge lengths of 15 mm, widths of 4 mm and thickness of 2 mm were cut along the extrusion direction (ED) and then polished by metallographic sandpaper. All specimens were tested with a speed of 0.5 mm/min, and the ductility was measured by extensometer.

3. Results and Discussion

In order to identify the phases clearly, the SEM and XRD of the pre-sintered and as-extruded composites are shown in Figure 1. According to XRD in Figure 1a,b, the composites contained TiB, α-Ti and β-Ti. Noting that no TiB_2 was detected, indicating that most of TiB_2 were reacted with Ti to produce TiB. Ma et al. [18] reported that when the ratio of B atoms below 49% to 50 at %, Ti atom would react with TiB_2 to form TiB. The phases composition, morphology and distribution were studied by the SEM in Figure 1c–f. According to the SEM images, TiBw, β-Ti and α-Ti were identified. During pre-sintering, TiBw emerged in the β grains boundaries. After extrusion, the sizes of TiBw increased and distributed along the ED. Meanwhile, the average sizes of β grains increased with the increasing extrusion temperature.

The inverse pole figure (IPF) mapping of as-extruded alloys and composites are shown in Figure 2. The black lines represent high-angle grain boundaries (HAGBs with misorientations > 15°), and the white lines represent low-angle grain boundaries (LAGBs with misorientations between 2° and 15°) [16,19]. The red lines distributed around phases, including α phase and TiBw. The coarse elongated β grains distributed along ED. Meanwhile, a large volume fraction of fine equiaxed β grains distributed inhomogeneously between elongated β grains, indicating dynamic recrystallization (DRX) occurred during extrusion [20,21]. Some β gains were distributed around TiBw and elongated α grains, typically as indicated by the black ellipse. Moreover, the necklace structure was distributed along the grain boundaries of elongated β grains, consisting of fine β grains and bulged HAGBs, as shown in the white ellipse. During deformation, the bulging grain boundaries severed as the nucleus of recrystallized grains, and recrystallized grains grew with the migration of HAGBs, resulting in necklace structure (DRX process on the bulged grain boundaries), that is discontinuous dynamic recrystallization (DDRX) [22].

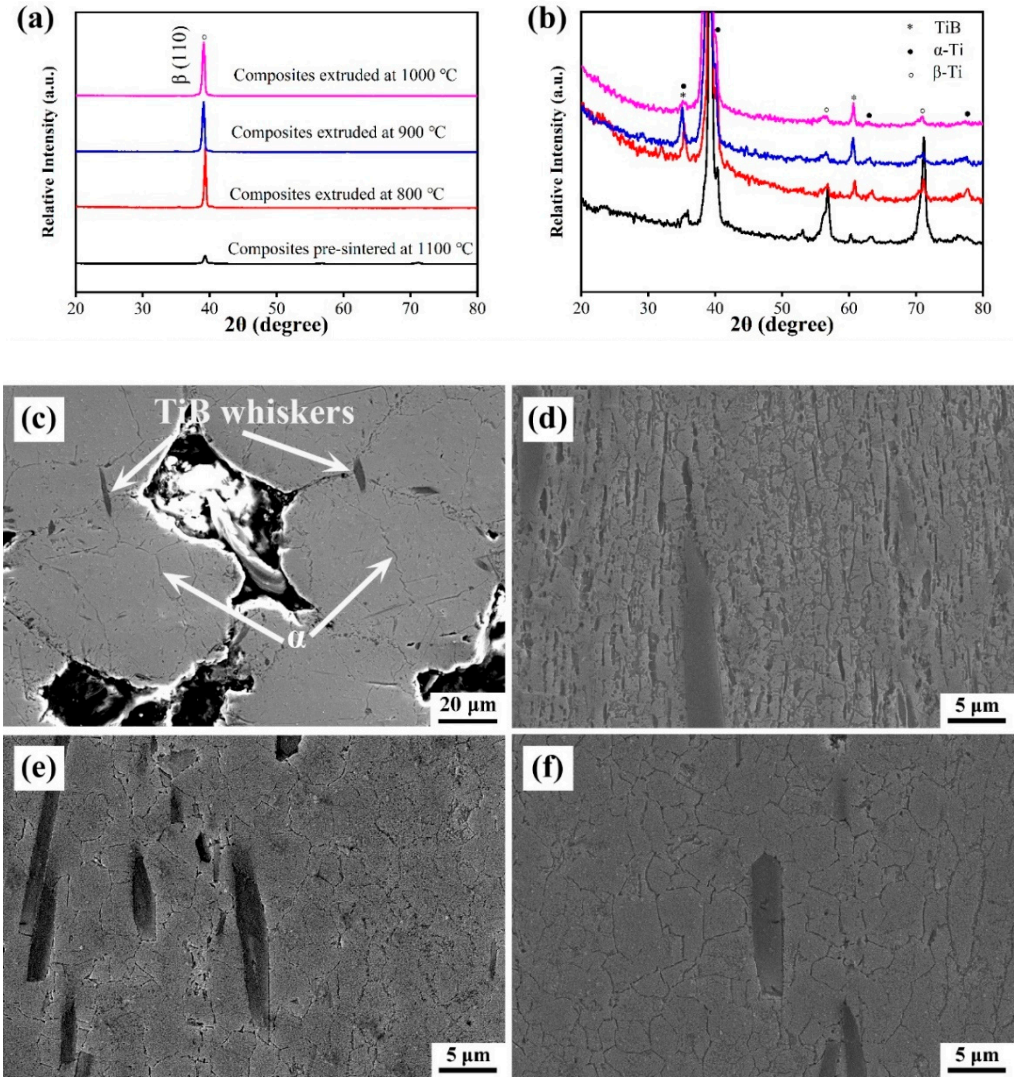

Figure 1. The XRD of pre-sintered and as-extruded composites (**a**), high magnification of XRD (**b**); SEM images of pre-sintered composites (**c**), composites extruded at 800 °C (**d**), composites extruded at 900 °C (**e**), composites extruded at 1000 °C (**f**).

In order to detect the orientation and texture of as-extruded alloys and composites, the discrete plot and texture along ED of alloys and composites extruded at 800 °C were shown in Figure 3a,b. The basal planes {0001} of α grains (⟨$2\bar{1}\bar{1}0$⟩ (point A1) and ⟨$10\bar{1}0$⟩ (point A3)) almost paralleled to ED, which contributed to ⟨$2\bar{1}\bar{1}0$⟩ α texture in Figure 3a,b and ⟨$10\bar{1}0$⟩ α texture in Figure 3b. During deformation, the prismatic glide of primary α grains (α_p) is {$10\bar{1}0$} ⟨$11\bar{2}0$⟩ [16]. Therefore, the basal planes {0001} of α_p would turn to parallel to ED. The α grain (⟨$10\bar{1}1$⟩ (point A2)) contributed to another center of α texture, which nucleated in the grain boundaries and grains according to the Burgers relationship {0001}//{110} and ⟨111⟩//⟨$11\bar{2}0$⟩ during β → α process [23]. Moreover, ⟨101⟩ β texture was maximum center in Figure 3a,b, which was commonly found in the fully recrystallized β grains of the deformed β phase due to the orientated nucleation mechanism [24,25].

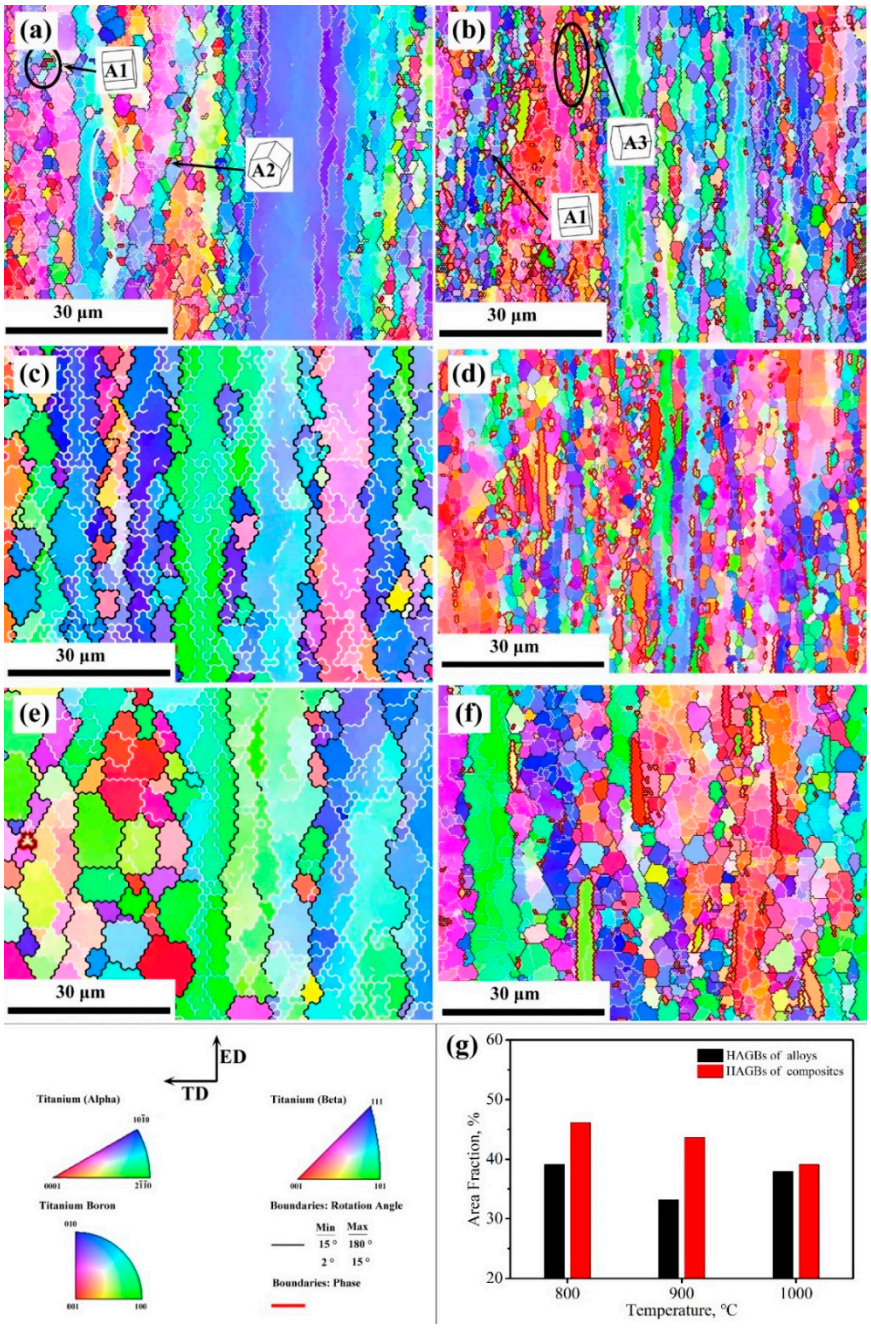

Figure 2. IPF mapping of alloys extruded at (**a**) 800 °C, (**c**) 900 °C, (**e**) 1000 °C and composites extruded at (**b**) 800 °C, (**d**) 900 °C, (**f**) 1000 °C; (**g**) histogram high-angle grain boundaries (HAGBs) counts of as-extruded alloys and composites.

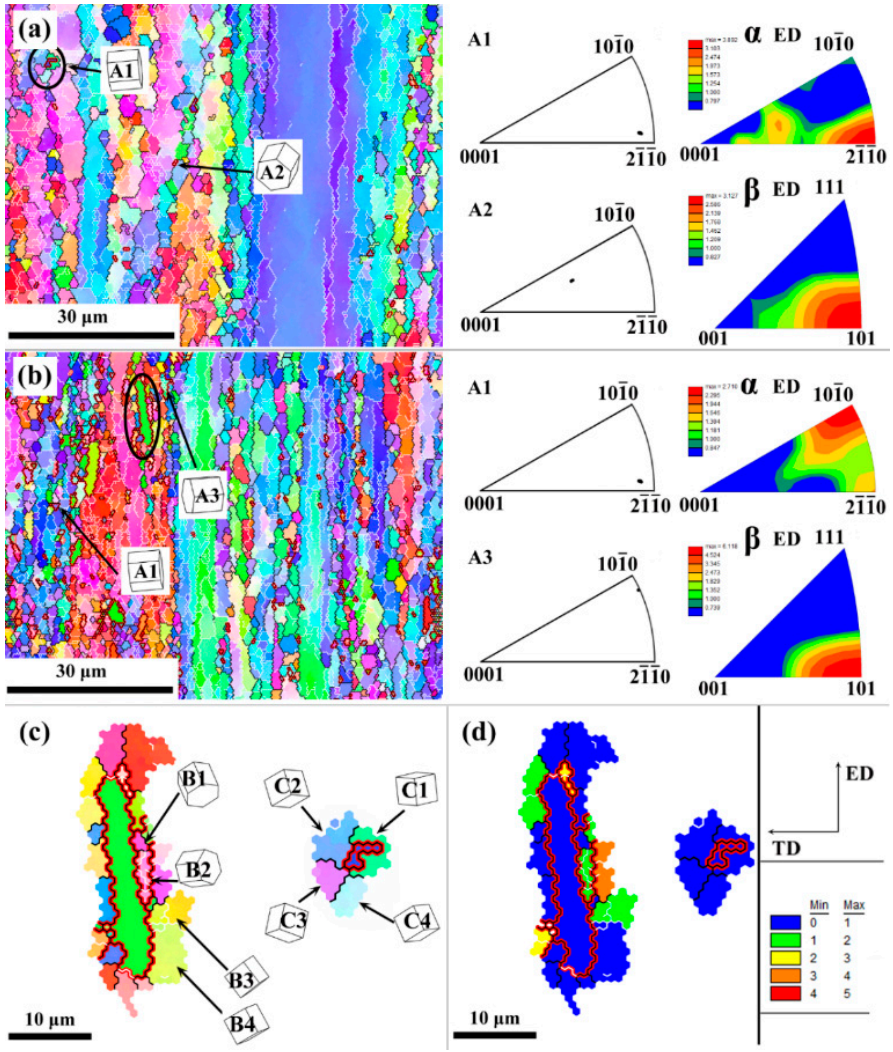

Figure 3. (**a**) IPF mapping, discrete plot and texture of alloy extruded at 800 °C; (**b**) IPF mapping, discrete plot and texture along extrusion direction (ED) of composite extruded at 800 °C; (**c**) highlighted mapping of (**a**,**b**); (**d**) grain orientation spread (GOS) mapping of (**c**).

The IPF and grain orientation spread (GOS) mapping of marked TiBw and α_p in Figure 3a,b are shown in Figure 3c,d. From Figure 3c, TiBw was surrounded by α grains and equiaxed β grains. Meanwhile, the GOS values of them are shown in Figure 4d. Basu et al. [26] revealed that the GOS values of the recrystallized grains were less than 1°, indicating β grains with blue color occurred DRX in Figure 3d. TiBw was a brittle phase with high elastic modulus, resulting in inharmonious deformation [27]. During extrusion, TiBw rotated to parallel to ED with the metal flow, and high extrusion stress concentrated around them by inharmonious deformation [24]. TiBw hindered dislocations motion, resulting in the piled up of dislocation around TiBw, which had been revealed by Park [28]. LAGBs emerged in the adjacent grains (point B2) and transformed into subgrains (point B3) with the accumulation of driving force. Subgrains rotated and formed equiaxed grains as further deformation, resulting in continuous dynamic recrystallization (CDRX) [25]. Meanwhile, the LAGBs evolved into HAGBs, which could be proved by the HAGBs volume fraction of composites increased by TiBw in Figure 2g. It should be pointed out that equiaxed β subgrains (point B4) occurred partial dynamic recrystallization without sufficient driving force [25]. A similar phenomenon was observed in Figure 2b,d,f, which may be attributed to a small rotation angle of TiBw.

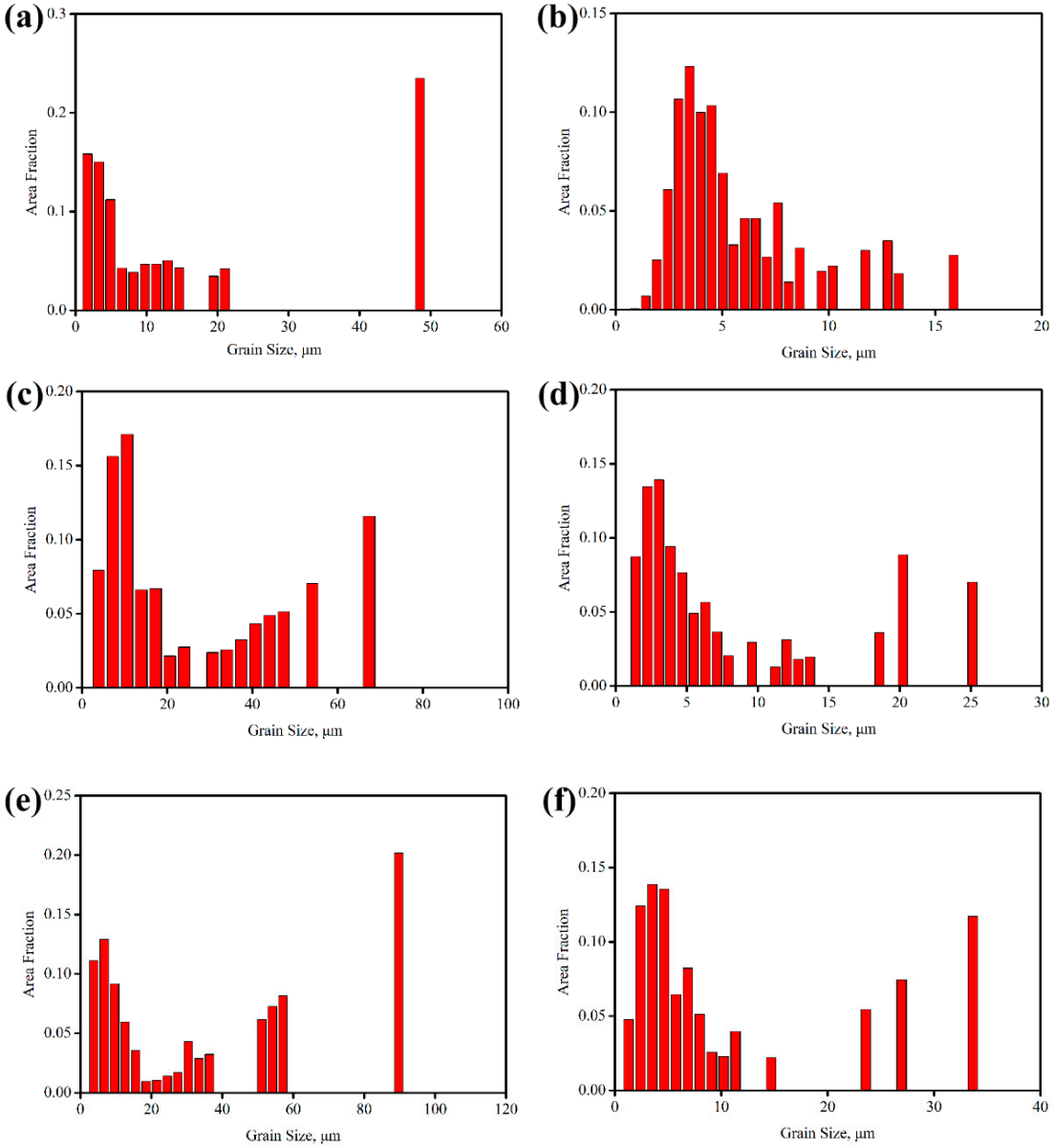

Figure 4. Histogram size counts of (**a**) alloys extruded at 800 °C, (**b**) composites extruded at 800 °C, (**c**) alloys extruded at 900 °C, (**d**) composites extruded at 900 °C, (**e**) alloys extruded at 1000 °C, (**f**) composites extruded at 1000 °C.

During extrusion at 800 °C, the basal planes {0001} of α_p would rotate to parallel to ED with the metal flow [24]. Meanwhile, the slip systems of α were limited with a hexagonal crystal structure (HCP), which led to inharmonious deformation. The relative high dislocation density would be accumulated in the grain boundaries between adjacent β grains and α_p [20], and the dislocation substructure formed [29]. The LAGBs in the adjacent β grains were contributed from the dislocation substructure slip and transformed into subgrains with the accumulation of deformation. Finally, the subgrains rotated and formed fine equiaxed β grains as further deformation, resulting in equiaxed β grains with random orientation (point C1, C2, C3, C4) [30]. Meanwhile, the LAGBs evolved into HAGBs, which also could be proved by that the HAGBs volume fraction of alloys reduced as α_p disappeared by extrusion temperature increased from 800 °C to 900 °C in Figure 2g.

The grain sizes distribution of alloys and composites extruded at different temperatures were shown by a histogram, as shown in Figure 4. The average sizes of β grains reduced obviously with the

precipitation of TiBw, particularly the volume fraction of β grains less than 10 μm increased obviously. Moreover, the average sizes of β grains increased with the increasing of extrusion temperature, resulting from more energy was obtained to promote the migration of grain boundaries for DDRX and growth with higher extrusion temperature [25]. During deformation, the rotation of TiBw promoted CDRX of β grains in inharmonious deformation, and the growth of CDRXed β grains was strongly inhibited by them, resulting in the higher volume fraction of fine β grains. Noting that coarse elongated β grains were shown in Figure 2. Figure 4 shows the sizes of coarse grains increased with the increasing extrusion temperature, resulting from the migration of grain boundaries promoted by more energy. The DDRXed and CDRXed β grains and coarse elongated β grains were attributed to bimodal grain size distribution in Figure 4 [31].

The room temperature tensile curves of alloys and composites extruded at 800, 900 and 1000 °C are shown in Figure 5a,b. The tensile strength of alloys decreases from 1086 MPa to 925 MPa with the increasing of extrusion temperature. During a tensile test, α_p distributed along grain boundary trapped dislocation for strengthening, which had been revealed by Liu [32]. Meanwhile, small grains were beneficial for strengthening effect [19]. In a word, when the alloy was extruded at 800 °C, α_p and refined grains contributed mainly for strengthening, with a strength of 1086 MPa. Meanwhile, α_p triggered massive stress concentration and served a nucleation of crack [32], which led to fracture, with 3.5% elongation.

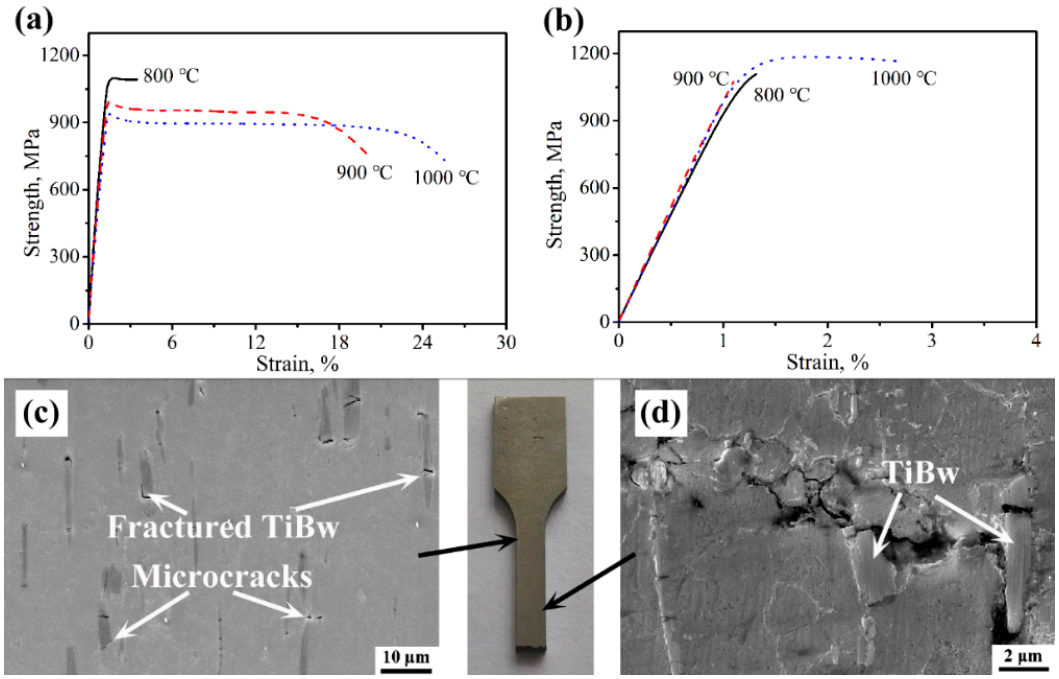

Figure 5. Room temperature tensile curves of (**a**) alloys extruded at 800, 900 and 1000 °C, (**b**) composites extruded at 800, 900 and 1000 °C; SEM of the longitudinal sections of the tensile test specimen of composites extruded at 1000 °C far away from the fracture surface (**c**), near the fracture surface (**d**).

During a tensile test for composites, the stress transfers from the matrix to TiBw due to inharmonious deformation, resulting in strengthening [27]. The findings for the composites extruded at 1000 °C will be discussed in the following in more detail and in Figure 5c,d [5]. Massive fractured TiBw and microcracks around TiBw were shown in the SEM image (Figure 5c) far away from the fracture surface., and the crack path included lots of cracks along TiBw and β grains boundaries in the SEM image (Figure 5d) near the fracture surface. These observations indicate that TiBw fractured with the accumulation of load transfer due to the inherent brittleness of TiBw [17], and then, microcracks emerged in the interface of TiBw and matrix. With further deformation, the cracks extended from

microcracks to the β grains boundaries of Ti matrix, leading to the final fracture. When the composite was extruded at 1000 °C, TiBw and grain refinement contributed for strengthening, with a strength of 1200 MPa, raising 27.9%.

4. Conclusions

In this work, the grain refinement and strengthening of TiBw/Ti-15Mo-3Al-2.7Nb-0.2Si alloy fabricated by powder metallurgy and canned hot extrusion were studied. The following conclusions were drawn:

(1) The β grains of composites were refined with the rotation and inhibition of TiBw. In inharmonious deformation, the dislocation motion was inhibited by TiBw, and CDRX of β grains was promoted with the rotation of TiBw. Meanwhile, the growth of CDRXed β grains was strongly inhibited.

(2) During extrusion below β phase region, the basal planes {0001} of α_p rotated to parallel to ED, resulting in grain refinement. The high dislocation density was accumulated in α_p grain boundaries, and inharmonious deformation supplied driving force to promote CDRX of adjacent β grains. Meanwhile, α_p slipped along the prismatic glide of $\{10\bar{1}0\}\langle 11\bar{2}0\rangle$, resulting in $\langle 2\bar{1}\bar{1}0\rangle$ and $\langle 10\bar{1}0\rangle$ α texture.

(3) The strength of composites extruded at 1000 °C was improved. TiBw loaded the stress transmitted from matrix until fracture, and grain refinement contributed to strengthening. Meanwhile, the microcracks initiated from the fractured TiBw.

Author Contributions: Conceptualization, J.H. and G.C.; methodology, L.G.; software, W.C.; validation, G.C., W.Z. and W.T.; investigation, L.G.; resources, W.Z.; data curation, L.G.; writing—original draft preparation, J.H. and L.G.; writing—review and editing, G.C., W.Z. and W.T.; project administration, W.Z.; funding acquisition, G.C. All authors have read and agree to the published version of the manuscript.

Funding: This research was funded by the Sci-tech Major Project in Shandong Province, grant number 2018GGX102013.

Conflicts of Interest: The authors declare no conflict of interest.

References

1. Zheng, Y.; Williams, R.E.; Wang, D.; Shi, R.; Nag, S.; Kami, P.; Sosa, J.M.; Banerjee, R.; Wang, Y.; Fraser, H.L. Role of ω phase in the formation of extremely refined intragranular α precipitates in metastable β-titanium alloys. *Acta Mater.* **2016**, *103*, 850–858. [CrossRef]
2. Yao, T.; Du, K.; Wang, H.; Huang, Z.; Li, C.; Li, L.; Hao, Y.; Yang, R.; Ye, H. In situ scanning and transmission electron microscopy investigation on plastic deformation in a metastable β titanium alloy. *Acta Mater.* **2017**, *133*, 21–29. [CrossRef]
3. Xiao, J.; Nie, Z.; Tan, C.; Zhou, G.; Chen, R.; Li, M.; Yu, X.; Zhao, X.; Hui, S.; Ye, W. The dynamic response of the metastable β titanium alloy Ti-2Al-9.2 Mo-2Fe at ambient temperature. *Mater. Sci. Eng. A* **2019**, *751*, 191–200. [CrossRef]
4. Cherukuri, B.; Srinivasan, R.; Tamirisakandala, S.; Miracle, D.B. The influence of trace boron addition on grain growth kinetics of the beta phase in the beta titanium alloy Ti–15Mo–2.6Nb–3Al–0.2Si. *Scr. Mater.* **2009**, *60*, 496–499. [CrossRef]
5. Okulov, I.; Bönisch, M.; Okulov, A.; Volegov, A.; Attar, H.; Ehtemam-Haghighi, S.; Calin, M.; Wang, Z.; Hohenwarter, A.; Kaban, I. Phase formation, microstructure and deformation behavior of heavily alloyed TiNb-and TiV-based titanium alloys. *Mater. Sci. Eng. A* **2018**, *733*, 80–86. [CrossRef]
6. Okulov, I.; Kühn, U.; Marr, T.; Freudenberger, J.; Schultz, L.; Oertel, C.-G.; Skrotzki, W.; Eckert, J. Deformation and fracture behavior of composite structured Ti-Nb-Al-Co (-Ni) alloys. *Appl. Phys. Lett.* **2014**, *104*, 071905. [CrossRef]
7. Okulov, I.; Kühn, U.; Marr, T.; Freudenberger, J.; Soldatov, I.; Schultz, L.; Oertel, C.-G.; Skrotzki, W.; Eckert, J. Microstructure and mechanical properties of new composite structured Ti–V–Al–Cu–Ni alloys for spring applications. *Mater. Sci. Eng. A* **2014**, *603*, 76–83. [CrossRef]

8. Okulov, I.; Okulov, A.; Soldatov, I.; Luthringer, B.; Willumeit-Römer, R.; Wada, T.; Kato, H.; Weissmüller, J.; Markmann, J. Open porous dealloying-based biomaterials as a novel biomaterial platform. *Mater. Sci. Eng. C* **2018**, *88*, 95–103. [CrossRef]
9. Okulov, I.; Okulov, A.; Volegov, A.; Markmann, J. Tuning microstructure and mechanical properties of open porous TiNb and TiFe alloys by optimization of dealloying parameters. *Scr. Mater.* **2018**, *154*, 68–72. [CrossRef]
10. Okulov, I.; Soldatov, I.; Sarmanova, M.; Kaban, I.; Gemming, T.; Edström, K.; Eckert, J. Flash Joule heating for ductilization of metallic glasses. *Nat. Commun.* **2015**, *6*, 7932. [CrossRef]
11. Okulov, I.; Volegov, A.; Attar, H.; Bönisch, M.; Ehtemam-Haghighi, S.; Calin, M.; Eckert, J. Composition optimization of low modulus and high-strength TiNb-based alloys for biomedical applications. *J. Mech. Behav. Biomed. Mater.* **2017**, *65*, 866–871. [CrossRef] [PubMed]
12. Okulov, I.V.; Wendrock, H.; Volegov, A.S.; Attar, H.; Kühn, U.; Skrotzki, W.; Eckert, J. High strength beta titanium alloys: New design approach. *Mater. Sci. Eng. A* **2015**, *628*, 297–302. [CrossRef]
13. Okulov, I.; Bönisch, M.; Volegov, A.; Shahabi, H.S.; Wendrock, H.; Gemming, T.; Eckert, J. Micro-to-nano-scale deformation mechanism of a Ti-based dendritic-ultrafine eutectic alloy exhibiting large tensile ductility. *Mater. Sci. Eng. A* **2017**, *682*, 673–678. [CrossRef]
14. Zhang, W.; Wang, M.; Chen, W.; Feng, Y.; Yu, Y. Evolution of inhomogeneous reinforced structure in TiBw/Ti-6AL-4V composite prepared by pre-sintering and canned β extrusion. *Mater. Des.* **2015**, *88*, 471–477. [CrossRef]
15. Wang, B.; Huang, L.J.; Liu, B.X.; Geng, L.; Hu, H.T. Effects of deformation conditions on the microstructure and substructure evolution of TiBw/Ti60 composite with network structure. *Mater. Sci. Eng. A* **2015**, *627*, 316–325. [CrossRef]
16. Feng, Y.; Zhang, W.; Cui, G.; Wu, J.; Chen, W. Effects of the extrusion temperature on the microstructure and mechanical properties of TiBw/Ti6Al4V composites fabricated by pre-sintering and canned extrusion. *J. Alloy. Compd.* **2017**, *721*, 383–391. [CrossRef]
17. Okulov, I.; Sarmanova, M.; Volegov, A.; Okulov, A.; Kühn, U.; Skrotzki, W.; Eckert, J. Effect of boron on microstructure and mechanical properties of multicomponent titanium alloys. *Mater. Lett.* **2015**, *158*, 111–114. [CrossRef]
18. Ma, X.; Li, C.; Du, Z.; Zhang, W. Thermodynamic assessment of the Ti–B system. *J. Alloy. Compd.* **2004**, *370*, 149–158. [CrossRef]
19. Dyakonov, G.; Mironov, S.; Semenova, I.; Valiev, R.; Semiatin, S. EBSD analysis of grain-refinement mechanisms operating during equal-channel angular pressing of commercial-purity titanium. *Acta Mater.* **2019**, *173*, 174–183. [CrossRef]
20. Lin, P.; Sun, Y.; Zhang, S.; Zhang, C.; Wang, C.; Chi, C. Microstructure and texture heterogeneity of a hot-rolled near-α titanium alloy sheet. *Mater. Charact.* **2015**, *104*, 10–15. [CrossRef]
21. Su, J.; Sanjari, M.; Kabir, A.S.H.; Jung, I.-H.; Yue, S. Dynamic recrystallization mechanisms during high speed rolling of Mg–3Al–1Zn alloy sheets. *Scr. Mater.* **2016**, *113*, 198–201. [CrossRef]
22. Belyakov, A.; Sakai, T.; Miura, H.; Kaibyshev, R.; Tsuzaki, K. Continuous recrystallization in austenitic stainless steel after large strain deformation. *Acta Mater.* **2002**, *50*, 1547–1557. [CrossRef]
23. Wang, S.C.; Aindow, M.; Starink, M.J. Effect of self-accommodation on α/ α boundary populations in pure titanium. *Acta Mater.* **2003**, *51*, 2485–2503. [CrossRef]
24. Huang, G.; Han, Y.; Guo, X.; Qiu, D.; Wang, L.; Lu, W.; Zhang, D. Effects of extrusion ratio on microstructural evolution and mechanical behavior of in situ synthesized Ti-6Al-4V composites. *Mater. Sci. Eng. A* **2017**, *688*, 155–163. [CrossRef]
25. Doherty, R.D.; Hughes, D.A.; Humphreys, F.J.; Jonas, J.J.; Rollett, A.D. Current issues in recrystallization: A review. *Mater. Sci. Eng. A* **1997**, *238*, 219–274. [CrossRef]
26. Basu, I.; Al-Samman, T. Twin recrystallization mechanisms in magnesium-rare earth alloys. *Acta Mater.* **2015**, *96*, 111–132. [CrossRef]
27. Panda, K.B.; Chandran, K.S.R. First principles determination of elastic constants and chemical bonding of titanium boride (TiB) on the basis of density functional theory. *Acta Mater.* **2006**, *54*, 1641–1657. [CrossRef]
28. Park, J.G.; Keum, D.H.; Lee, Y.H. Strengthening mechanisms in carbon nanotube-reinforced aluminum composites. *Carbon* **2015**, *95*, 690–698. [CrossRef]

29. Murty, S.V.S.N.; Nayan, N.; Kumar, P.; Narayanan, P.R.; Sharma, S.C.; George, K.M. Microstructure–texture–mechanical properties relationship in multi-pass warm rolled Ti–6Al–4V Alloy. *Mater. Sci. Eng. A* **2014**, *589*, 174–181. [CrossRef]
30. Dong, R.; Li, J.; Kou, H.; Tang, B.; Hua, K.; Liu, S. Characteristics of a hot-rolled near β titanium alloy Ti-7333. *Mater. Charact.* **2017**, *129*, 135–142. [CrossRef]
31. He, J.; Jin, L.; Wang, F.; Dong, S.; Dong, J. Mechanical properties of Mg-8Gd-3Y-0.5 Zr alloy with bimodal grain size distributions. *J. Magnes. Alloy.* **2017**, *5*, 423–429. [CrossRef]
32. Liu, C.; Lu, Y.; Tian, X.; Liu, D. Influence of continuous grain boundary α on ductility of laser melting deposited titanium alloys. *Mater. Sci. Eng. A* **2016**, *661*, 145–151. [CrossRef]